Journal of Applied Automation Technologies

Research Paper

# State-Space Refined Kalman Filter Model for Battery State-of-Health Estimation in Energy Storage Power Stations

**Adam Kacper Dmochowski[1] and Ludwik Kostecki[1, *]**

[1] Faculty of Automation & Electrical Engineering, State Higher School in Walcz, Walcz, 78-600, Poland
*Corresponding author: ludwik.k@pwsz-walcz.edu.pl

**Abstract.** Numerous issues, including partial cycling, current pulses, thermal gradients, and module anomalies, affect battery state-of-health estimation in grid energy storage systems. In this research, develop a state-space refined Kalman filter model that interprets resistance increase and capacity loss as slowly changing states instead of post-processed indications. Temperature-normalized ageing drift, innovation-governed covariance inflation, and a station-level consistency requirement are combined with a second-order equivalent-circuit representation. Twelve integrated sensors gathered temperature data and over 214 operation days of 18,640 charge-discharge fragments from nine-six lithium iron phosphate cells arranged into eight 52 V modules. The state-of-health mean absolute errors were lowered to 1.18%, 1.91%, and 2.78%, respectively, by using a dual Kalman filter and a recursive least squares baseline in place of the traditional extended Kalman filter. The variance in capacity estimation for operation at 0.2C to 1.0C has decreased by 31.7%, and the 95th percentile error has decreased to 2.64%. Additionally, the estimator can identify the high-temperature rack's accelerated degradation 17 days ahead of the baseline alert rule. The findings suggest that, without the use of black-box features, explicit state-space modification can improve the model's accuracy, stability, and engineering interpretability.

**Keywords:** *Kalman Filtering, State Space Refinement, Battery State of Health, Covariance Inflation, Equivalent Circuit Model*

Received on 16 February 2023, Accepted on 18 July 2023, Published on 29 July 2023



## Introduction

Large-scale electrochemical energy storage facilities are now used to buffer the volatility of intermittent renewable energy sources and power-system dispatch, but they are less reliable because the battery packs have aged under conditions of infrequent use. Lithium iron phosphate batteries in a grid service application may show temperature drift during standby, shallow cycling at noon, pulse discharge during nocturnal peak, and sporadic high-current balancing activities. As the two regimes change the relationship among voltage response, available capacity and internal resistance, a health index that is suitable in one set of circumstances may not be suitable in another [1]. Therefore, the operator's maintenance schedule module needs high-accuracy prognostics and health management (PHM) technology that engineers can understand [2]. Traditional capacity evaluations are rarely feasible at the station level and during stop service [3]. Voltage-type indicators are simple to use but are also sensitive to the history of current and relaxation time [4]. There are other reasons for the drop in usable capacity, and even if the rise in resistance is more pronounced during the pulse, it may still be the same as [5]. A data-driven predictor can learn the complex pattern from many labelled examples; however, the storage station only has some operational data that lacks health labels [6]. Model-based filtering strategies have been proposed to connect the quantifiable electrical signal with the hidden degradation state [7]. The estimator should also be numerically stable after an abrupt change in dispatch [8].

Kalman filtering has been applied to battery management in recent years due to its recursive characteristics and suitability for equivalent-circuit modeling in the propagation of uncertainty. Periodically adjust the capacity or find other factors to estimate the relevant health value, and use a relatively quick estimation method for the

https://doi.org/10.64972/jaat.2023v1.302p16e:213-227

state of charge [9]. The Gap has weakened the connection between short-term electrical behaviour and long-term degradation. Use two filters to obtain both the state and the parameter at the same time [10]; modify the filter covariance to address anomalous measurement residuals [11]. If the current excitation is too low, the augmented model may be ill-conditioned; joint estimators can add resistance or capacity as enhanced states [12]. Sensor offsets, temperature-accelerated aging, uneven packing and insufficient rest intervals are also problems at the energy storage station [13]. Based on the engineering analysis in [14], although the equivalent-circuit filter performed well in the controlled experiment, it drifted over time during actual dispatch. Therefore, the practical estimator should restrict the state space to one that is still physically meaningful, avoid having too many parameter freedoms, and use innovation information for adaptation under different operating conditions [15].

A State-Space Refined Kalman Filter Model for Battery Health Estimation in Energy Storage Power Stations is presented in this paper. In short, it is a slow-changing, direct-measurement index of health that is linked to module-level consistency, ohmic resistance, polarization dynamics, temperature-normalized stress, and usable capacity. We have included degradation-sensitive variables in a compact state equation and employed innovation statistics to handle uncertainty under non-standard cycling conditions, thus avoiding the use of a black-box learner for electrochemical knowledge. This paper first introduces the improved model and then presents some examples of estimating techniques, state construction, transition design, measurement coupling and covariance regulation. The performance of the suggested filter is evaluated based on a station-like dataset of lithium iron phosphate at different currents, temperatures and aging stages, and several representative baseline models are presented in the experimental section.

## Related Work

### Model-Based Battery Health Estimation

Most of the model-based health estimates start with an electrochemical or equivalent-circuit model and then extract parameters related to degradation. As their voltage equations can be obtained online with only a few sensors, equivalent-circuit models have been applied widely [16]. First-order resistor-capacitor models are computationally simple, but their charge-transfer and diffusion behaviour can be incorporated into a single polarisation term [17]. A pulse response has both a quick and a slow relaxation component, so a second-order circuit is relatively suitable for the station battery [18]. Although they are more difficult to recognise in the case of irregular dispatch, electrochemical reduced-order models have a greater physical meaning [19]. Although capacity and internal resistance have been used as health indicators in some studies, the effect of changes in temperature, rest time and current amplitude on these two categories is not the same [20].

Online find the circuit parameters and then determine the health based on experimental relationships; this is a typical engineering approach. Given the above, this estimator is relatively simple; however, it generally treats health as an end state rather than an object of inquiry over time. A shift in the operating point may result in a health oscillation due to transiently absorbing the unmodeled voltage error. Because the cells in the same rack may have different thermal and balancing histories, the energy storage station is more likely to have this problem. Therefore, the state formulation for health estimation must limit the freedom of weakly observable characteristics and connect degradation with the electrical response.

### Kalman Filtering and Adaptive Fusion

Extended Kalman filters, Unscented Kalman filters, dual Kalman filters and adaptive covariance variants are all examples of Kalman-filter-based battery estimation. The voltage equation is nonlinear; therefore, an extended Kalman filter is used to linearize it around the current operating point for estimation [21]. Although unscented Kalman filtering has a relatively high processing cost for large module groups, it can deal with non-linear propagation without explicitly generating the Jacobian [22]. Dual Kalman filtering is suitable for cases where the capacity and resistance wander slowly with charge movement because it separates state and parameter estimation [23]. Adaptive covariance rules increase the uncertainty of anomalous residuals in a period to enhance robustness [24]. Voltage, current, temperature and operating environment data are added by combining multiple sources; however, features that cannot be trusted due to noisy or missing sensing should not be generated [25].

https://doi.org/10.64972/jaat.2023v1.302p16e:213-227

Recursive estimation is suitable for online battery management, and although some filtering studies have been conducted, many problems remain at the station-level health assessment. First, the response to actual deterioration is delayed, and health is often repaired outside of the state equation. Second, covariance adaptation frequently fails to consider current excitation, temperature stress and module consistency, and is only triggered by a certain amount of the residual. Third, although many studies have shown good accuracy for standard cycle profiles, they have provided little data in the event of partial charging, current pulses, or extended idle periods. The engineering domain we are concerned with here is defined by the deficiencies: a compact state-space refinement that enhances accuracy under stationarity and maintains the interpretability of filters.

The purpose of the estimation is also an applied problem. A filter can be used to modify the terminal voltage by changing the state of charge or polarisation and biasing the degradation; therefore, a low-voltage residual does not always indicate poor health. However, unless a capacity check reveals a drift, a health estimate that is too smooth and insensitive to the current excitation may appear reasonable. Therefore, in the engineering review, health errors, residual structures, uncertainty behaviour and warning stability all need to be considered. In this study, the experiment has been extended to include, among others, the average error, percentile error, transient recovery, temperature sensitivity and alarm lead time of the proposed model.

## Refined State-Space Kalman Filtering Model

### State Construction and Degradation Coupling

In Figure 1, the proposed estimator uses a second-order equivalent-circuit model and augments its fast electrical states with slow degradation states. The state vector contains state of charge $z_k$, two polarization voltages $v_{1,k}$ and $v_{2,k}$, available capacity $Q_k$, ohmic resistance $R_{0,k}$, and state of health $h_k$. The health state is not computed only after filtering; it is included in the transition model and corrected by voltage innovation. shows the estimator architecture and the information flow from station sensors to module-level health output.

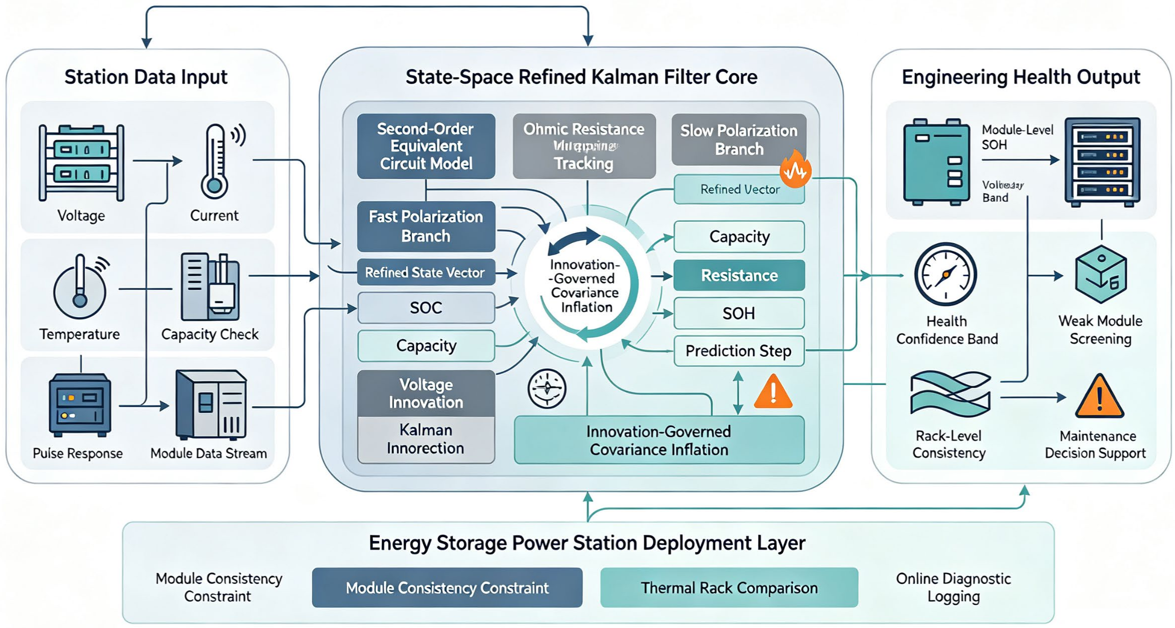


**Figure 1.** For the proposed state-space refined Kalman filter architecture.

The refined state vector is defined as a compact group of electrical and degradation variables:

$$x_k = [z_k, v_{1,k}, v_{2,k}, Q_k, R_{0,k}, h_k]^T \qquad \text{Eq.(1)}$$

In this expression, $x_k$ is the complete hidden state at sampling instant $k$. The first three entries describe short-time electrical behavior, while $Q_k$, $R_{0,k}$, and $h_k$ describe slow aging. This arrangement lets the Kalman correction update health only when the voltage residual remains meaningful after fast polarization has been explained.

The state-of-charge transition follows coulomb counting with capacity feedback, where $I_k$ is positive during discharge, $\eta$ is coulombic efficiency, and $\Delta t$ is the sampling interval:

$$z_{k+1} = z_k - \frac{\eta I_k \Delta t}{Q_k} + w_{z,k} \quad \text{Eq.(2)}$$

This expression avoids propagating state of charge with a fixed rated capacity. When $Q_k$ declines, the same current produces a larger change in $z_k$, which is exactly what an aged module exhibits. The noise term $w_{z,k}$ absorbs currentsensor bias, integration error, and small coulombic-efficiency deviations.

The two polarization voltages follow discrete resistor-capacitor dynamics with different time constants:

$$v_{i,k+1} = \exp\left(-\frac{\Delta t}{R_i C_i}\right) v_{i,k} + R_i \left(1 - \exp\left(-\frac{\Delta t}{R_i C_i}\right)\right) I_k + w_{i,k}, i = 1,2 \quad \text{Eq.(3)}$$

Here, $i = 1$ and $i = 2$ denote fast and slow polarization branches. The exponential coefficient preserves relaxation after current changes, while the second term converts current excitation into polarization voltage. Two branches prevent transient voltage sag from being incorrectly assigned to ohmic resistance and health loss.

Capacity and resistance are allowed to evolve slowly. Their drift terms are governed by temperature-normalized current stress $s_k$, which prevents ordinary current pulses from being interpreted as abrupt aging:

$$Q_{k+1} = Q_k - \alpha_Q s_k \Delta t + w_{Q,k} \quad \text{Eq.(4)}$$

In this expression, $\alpha_Q$ converts the stress index into capacity loss, and $w_{Q,k}$ represents unmodeled aging dispersion among cells. The negative sign constrains capacity to fade rather than fluctuate symmetrically. Because $s_k$ includes temperature normalization, hot high-current operation carries more aging weight than cool low-current operation.

The resistance transition uses the same stress indicator but permits asymmetric growth because resistance rise is more visible during high-current pulses:

$$R_{0,k+1} = R_{0,k} + \alpha_R s_k |I_k| \Delta t + w_{R,k} \quad \text{Eq.(5)}$$

This expression uses $|I_k|$ because charge and discharge pulses both expose impedance-related voltage drop. The coefficient $\alpha_R$ is kept conservative so that short pulses do not permanently inflate resistance. The noise term $w_{R,k}$ allows gradual rack-level divergence caused by temperature and balancing differences.

Health is represented as normalized usable capacity corrected by resistance growth, so it can react to both energy loss and power capability degradation:

$$h_k = \lambda_Q \frac{Q_k}{Q_0} + \lambda_R \frac{R_{0,0}}{R_{0,k}}, \lambda_Q + \lambda_R = 1 \quad \text{Eq.(6)}$$

Here, $Q_0$ and $R_{0,0}$ are the initial calibrated capacity and resistance, while $\lambda_Q$ and $\lambda_R$ determine the relative importance of energy capability and power capability. The weight constraint keeps $h_k$ normalized and interpretable. A health state that ignores resistance can remain optimistic during early impedance rise; a health state that overemphasizes resistance can become unstable during transient pulses.

The measurement equation links terminal voltage to open-circuit voltage, ohmic drop, and polarization response:

$$y_k = U_{\text{oc}}(z_k, T_k) - I_k R_{0,k} - v_{1,k} - v_{2,k} + e_k \quad \text{Eq.(7)}$$

This expression is the bridge between measurable station data and hidden health states. The measured voltage $y_k$ is explained by temperature-dependent open-circuit voltage, instantaneous ohmic loss, two polarization losses, and measurement noise $e_k$. Persistent residual bias after these terms is considered gives the filter stronger evidence for correcting degradation states.

**Prediction, Correction, and Innovation Regulation**

The nonlinear transition and measurement equations are locally linearized for recursive filtering. Let $f(\cdot)$ denote the state transition and $g(\cdot)$ denote the voltage measurement function. The predicted state and covariance are written as:

$$x_k^- = f(x_{k-1}^+, I_{k-1}, T_{k-1}) \quad \text{Eq.(8)}$$

The superscript minus denotes the prior estimate before the new voltage measurement is used, and the superscript plus denotes the corrected estimate from the previous step. This prediction carries the last accepted state through the physical transition model using current and temperature inputs. This prediction is where aging drift is introduced before measurement feedback arrives.

The corresponding covariance prediction uses the Jacobian $F_{k-1}$ and process-noise covariance $Q_{k-1}^{x}$ :

$$P_k^- = F_{k-1}P_{k-1}^+F_{k-1}^T + Q_{k-1}^x \qquad \text{Eq.(9)}$$

In this expression, $P_k^-$ quantifies uncertainty in the predicted state. The Jacobian $F_{k-1}$ propagates uncertainty through the locally linearized transition, while $Q_{k-1}^x$ adds uncertainty from unmodeled aging and sensor integration error. Larger degradation-state covariance makes the filter more willing to correct $Q_k$, $R_{0,k}$, and $h_k$.

The voltage innovation is the difference between the measured terminal voltage and the predicted voltage:

$$r_k = y_k - g(x_k^-, I_k, T_k) \qquad \text{Eq.(10)}$$

The innovation $r_k$ is the main diagnostic signal of the recursive estimator. A small random innovation means the predicted state explains the terminal voltage well. A persistent signed innovation indicates that the model is missing a voltage component, but the filter still checks operating current and covariance before treating that residual as aging evidence.

The Kalman gain uses the measurement Jacobian $H_k$ and measurement-noise covariance $R_k^y$ :

$$K_k = P_k^- H_k^T \left(H_k P_k^- H_k^T + R_k^y\right)^{-1} \qquad \text{Eq.(11)}$$

This expression determines how strongly the measurement should modify the predicted state. If measurement noise $R_k^y$ is large, the gain becomes smaller and the filter trusts the model more. If the predicted covariance is large and the voltage equation is sensitive to a state, the gain increases and that state receives a stronger correction.

The corrected state and covariance are obtained by standard recursive update:

$$x_k^+ = x_k^- + K_k r_k \qquad \text{Eq.(12)}$$

This expression applies the innovation-weighted correction to the whole state vector. The same residual can update state of charge, polarization voltages, resistance, capacity, and health, but the magnitude of each update is controlled by the corresponding gain entry. This is why physically meaningful covariance design is essential for health estimation.

A station-level dispatch sequence can cause residual bursts that are not aging events. The model therefore scales degradation-state covariance using an innovation score $\gamma_k$ computed over a sliding window:

$$\gamma_k = \frac{r_k^2}{H_k P_k^- H_k^T + R_k^y} \qquad \text{Eq.(13)}$$

The score $\gamma_k$ normalizes the squared innovation by its expected variance. A large residual is not automatically abnormal if the predicted uncertainty is also large. This normalized form helps distinguish ordinary model uncertainty from residual bursts that may contain useful information about degradation or sensor disturbance.

When $\gamma_k$ exceeds its expected range and current excitation is sufficient, covariance inflation is applied only to capacity, resistance, and health entries:

$$Q_k^x = Q_0^x + \beta \max\left(0, \gamma_k - \tau\right) D_h \qquad \text{Eq.(14)}$$

Here, $Q_0^x$ is the nominal process-noise covariance, $\beta$ controls the strength of inflation, $\tau$ is the innovation threshold, and $D_h$ selects only the degradation-related states. The term $\max(0, \gamma_k - \tau)$ prevents inflation when the innovation remains within the expected range. This makes the adaptation selective instead of allowing every voltage transient to loosen the entire filter.

This selective inflation is the main distinction between the proposed estimator and a generic adaptive filter. If the full covariance matrix is inflated, state of charge and polarization voltage may become unnecessarily noisy after every dispatch transition. If no inflation is used, the filter can become overconfident and reject genuine degradation evidence. The diagonal selector $D_h$ confines adaptation to the slow variables, while the innovation threshold prevents ordinary measurement noise from repeatedly widening the health uncertainty. In

https://doi.org/10.64972/jaat.2023v1.302p16e:213-227

implementation, the threshold is evaluated together with current magnitude and temperature validity, because a large residual during idle rest carries less health information than the same residual during a current pulse.

### Station-Level Consistency Constraint

Energy storage stations rarely operate isolated cells. The estimator therefore introduces a soft consistency constraint across modules in the same thermal rack. The constraint discourages physically unrealistic divergence while still allowing a genuinely weak module to separate from the group.

$$h_{k,c}^{m,+} = h_k^{m,+} - \rho\left(h_k^{m,+} - \mathrm{median}\left(h_k^{1:M,+}\right)\right) \quad \text{Eq.(15)}$$

In this expression, $h_k^{m,+}$ is the corrected health of module $m$, $h_{k,c}^{m,+}$ is the consistency-adjusted health, $M$ is the number of modules in the same comparison group, and $\rho$ is a small consistency coefficient. The median is used instead of the mean because it is less sensitive to one abnormal module or one temporary sensor fault. The correction is soft: when $\rho$ is close to zero, the module remains almost independent; when $\rho$ increases, unrealistic module separation is suppressed more strongly.

The consistency constraint is applied after the ordinary Kalman correction rather than before it. This ordering allows each module to use its own voltage, current, and temperature evidence first. The station-level correction then removes only the part of the health deviation that is inconsistent with neighboring modules under similar thermal and operating conditions. If a module remains lower than the rack median across repeated updates, the constraint does not erase the fault; it merely prevents a single noisy update from creating a false weak-module diagnosis.

The coefficient $\rho$ is selected according to the expected module dispersion of the station. A new station with tightly matched modules can use a slightly stronger constraint, while an aged station with known module imbalance should use a weaker value. In the experiments, $\rho$ is kept below 0.1 so that the correction changes health slowly compared with the Kalman update. This choice preserves fault observability while improving numerical stability during residual bursts.

From Figure 2, the overall implementation contains sensor screening, state prediction, voltage correction, innovation scoring, covariance regulation, and module consistency correction, gives the online workflow used in the experiments.

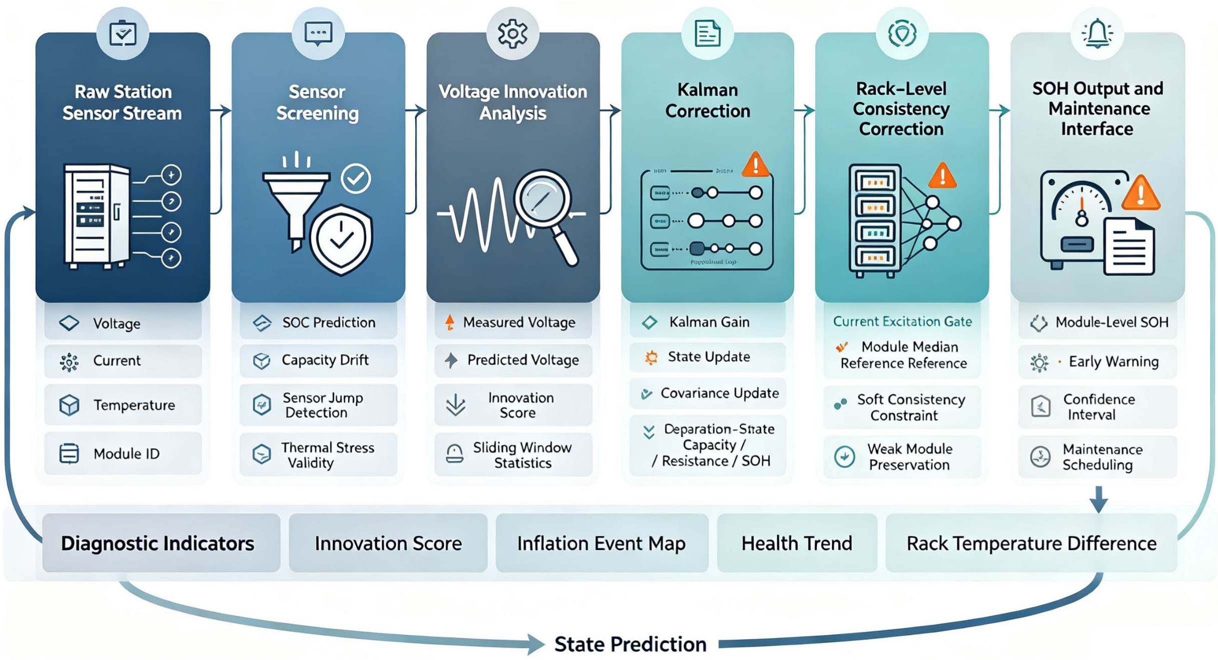


**Figure 2.** For the online estimation workflow from sensor screening to module-level state-of-health output.

The online workflow begins by screening voltage, current, and temperature samples for missing values and abrupt sensor jumps. The model then predicts each module state, computes the voltage innovation, updates the state with the Kalman gain, adjusts degradation covariance when the innovation score is meaningful, and finally applies the rack-level consistency rule. This sequence keeps local electrochemical evidence ahead of station-level smoothing, which is necessary for detecting a genuinely weak module.

The three parts of the model therefore play different roles. Section 3.1 defines the physical state variables and their degradation coupling. Section 3.2 specifies how those states are recursively corrected and how uncertainty is regulated. Section 3.3 adds the station-level engineering constraint required when many modules operate under shared dispatch and thermal conditions.

## Experimental Dataset and Performance Analysis

### Dataset, Operating Conditions, and Baselines

For the assessment, 96 lithium iron phosphate cells in eight modules provided station-like aging data. Each module features a temperature-varying cabinet, a pulse-power segment, a standby interval, 12 cells connected in series, and a partial charge-discharge cycle. After filtering, the 214-day record has 18,640 useable fragments. The ambient temperature range is 15.2°C to 39.6°C, the current range is 0.2°C to 1.0°C, and the measured module terminal voltage during active operation is collected every second. A 21- to 28-day schedule serves as the reference value for the low-current capacity check, which is solely interpolated for the error computation. Station diagnostic investigations employ the same engineering validation circumstances, and occasional load-labeling and partial cycling are inevitable [26].

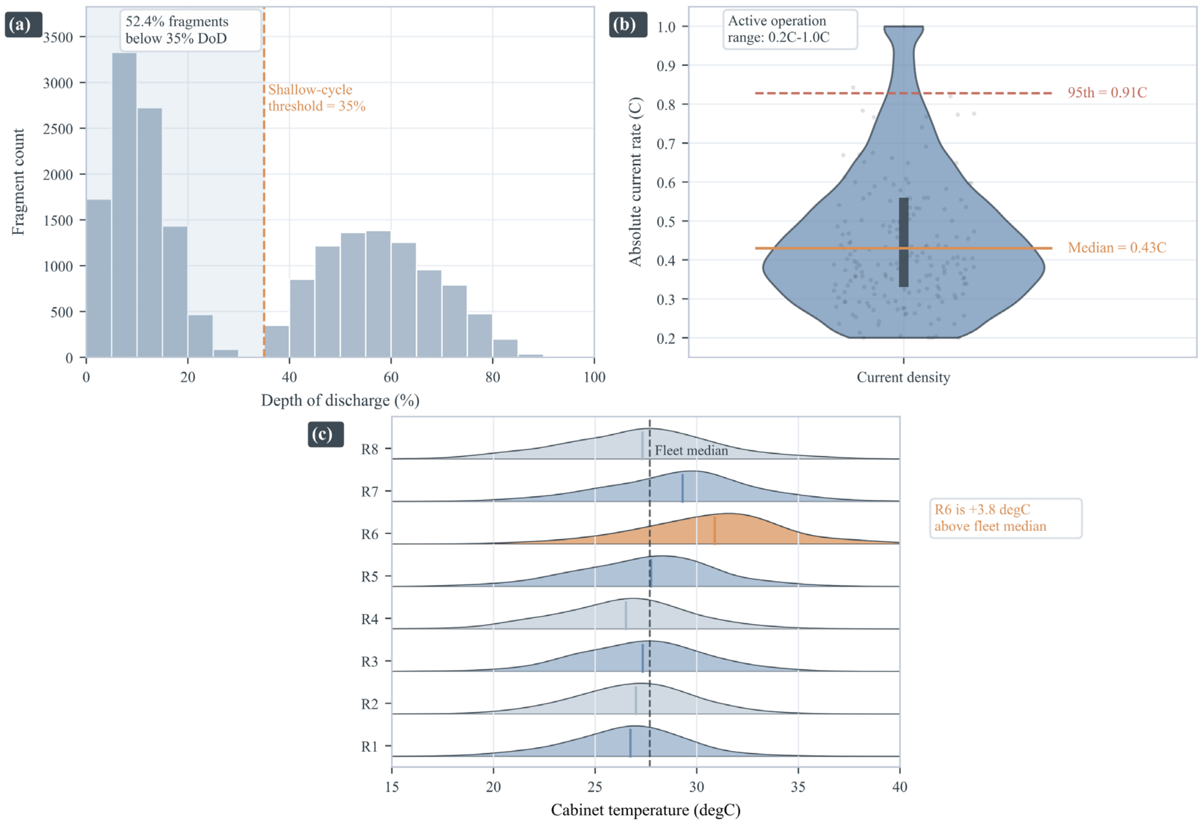


**Figure 3.** Placeholder for dataset characterization: (a) depth-of-discharge; (b) current-density; (c) temperature distribution.

Instead of being divided into random pieces, a dataset is divided by time. Initial parameter calibration will take place during the first 48 days, followed by filter tuning from day 49 to day 154 and the final test from day 155 to day 214. The estimator's future degradation patterns will not be displayed by this division. Three baselines are employed: a dual Kalman filter that estimates capacity in a parameter channel, a recursive least-squares estimator with voltage residual correction, and a conventional extended Kalman filter that predicts the state of charge before determining resistance. For Battery Management Systems (BMSs), the baselines are common engineering options [27]. The test record is shown in Figure 3. Figure 3(a) indicates that 52.4% of the fragments are shallow cycles below 35% depth of discharge; Figure 3(b) displays the current distribution, with a median absolute current of 0.43C and a 95th percentile of 0.91C; and Figure 3(c) displays the cabinet temperature distribution; during summer operation, rack R6 is 3.8°C warmer than the fleet median.

Module voltage, current, temperature, periodic capacity, and pulse-derived resistance are the five measured quantities that will be analyzed. To calculate the covariance inflation ratio and innovation score for use as internal diagnostic indicators, a model was put forth. The signs are able to differentiate between numerical problems and estimating errors. Following sensor screening, the initial state-of-health uncertainty is set to 3.0%, and the measurement-noise standard deviation is set to 7.5 mV. According to capacity inspections, the eight modules' health ranges from 91.7% to 95.8% at the conclusion and from 99.1% to 100.0% at the beginning. Thus far, the coldest module has lost 4.2% of its capacity and the warmest module has lost 7.4%; this is consistent with the thermal acceleration seen in the storage-station data [28]. The identical calibration and validation windows are also used by the baselines. In the conventional extended Kalman filter, health is deduced from the recognized capacity at certain checkpoints, and the process noise of the state of charge is selected to minimize the voltage root-mean-square residual. During times of low current, both Kalman filters decrease the parameter covariance and update the state and parameter channels simultaneously. Recursive Least Squares: The ideal validation value of 0.982 is obtained by varying the forgetting factor between 0.965 and 0.995. By not optimizing the suggested model while utilizing default baselines, the choices will prevent an irrational comparison.

**Estimation Accuracy and Robustness**

During the last test period, the suggested filter had the lowest overall error. Compared to the 2.36% of the traditional extended Kalman filter, the 1.91% of the dual Kalman filter, and the 2.78% of recursive least squares, the mean absolute state-of-health error for all modules is 1.18%. The corresponding root-mean-square errors are 1.47%, 2.91%, 2.38%, and 3.22%. Because the refined state vector does not exhibit a notable shift in resistance growth due to capacity loss, the gain is comparatively high on pulse-rich days. The model comparison is shown in Figure 4: (a) represents the mean absolute error of each module, and all eight modules of the proposed filter are less than 1.45%; Figure 4 (b) represents the 95th percentile error, which has decreased from 4.98% for the conventional filter to 2.64%; and Figure 4 (c) represents the cumulative absolute error, where the best baseline reaches 1,216 and the proposed curve reaches 752 percentage-point samples.

The distribution of the decreased mistakes is not uniform. Because the ohmic voltage loss is partially interpreted as a lower state of charge, the conventional filter exhibits a positive health bias of 2.1% in the 0.8C discharge stage. By combining resistance and health estimation, the suggested filter lowers the bias shown above to 0.6%. Because there is no voltage excitation for capacity correction during low-current standby recovery, the two filters have a slight capacity drift. Because the suggested innovation rule restricts the inflation of capacity covariance under weak excitation, its standby drift stays below 0.4% during a 36-hour period, which is less than the dual-filter's 1.3%. Filtering investigations thus demonstrate that identifiability in battery parameter estimation is dependent on excitation [29].

Results at the module level demonstrate that the suggested estimator is not restricted to the average of the modules. M1, M2 and M4 are near to the station's mean temperature, and their final-test mean absolute errors are 0.94%, 0.87% and 1.05%, respectively. M6 and M7 have a higher cabinet temperature and stronger balancing activity; their errors are 1.45% and 1.33%, respectively, and despite higher than the best baseline values of 2.14% and 2.02%, they are still lower. The single highest inaccuracy of the suggested model is 3.21%, and it comes immediately after a high-current discharge followed by a 19-minute rest period. The conventional filter in the same part has a 6.84% mistake because it temporarily underestimates the status of charge and overcorrects health. The improved filter does not remove all transitory mistakes, but it reduces the recovery time from 47 minutes to 11 minutes.

https://doi.org/10.64972/jaat.2023v1.302p16e:213-227

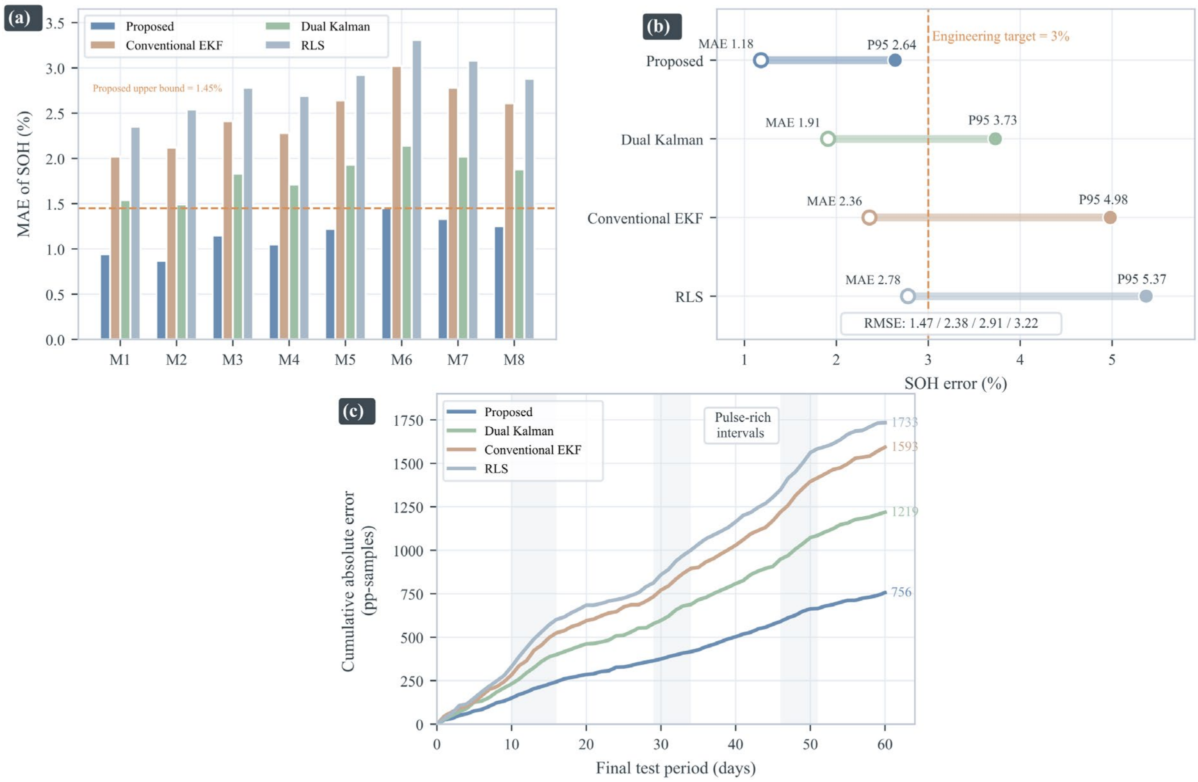


**Figure 4.** Placeholder for accuracy comparison: (a) module-wise MAE; (b) 95th-percentile error; (c) cumulative absolute error.

The voltage residual statistics are as follows: The proposed filter attained a terminal-voltage residual root-mean-square value of 13.6 mV in the test interval, and the conventional, dual and recursive baselines were 18.9 mV, 16.7 mV and 21.4 mV correspondingly. More importantly, the suggested filter's residual autocorrelation at a 60-second lag has decreased from 0.41 in the traditional filter to 0.18. Lower residual autocorrelation implies that the estimator has absorbed the systematic polarization and resistance behaviour and no longer considers it a structured voltage error. If the same dispatch pattern is repeated every day in the context of health estimate, structured residuals will accrue biased deterioration correction after a few days.

Voltage sensor offset, missing temperature measurements, and abrupt dispatch switching are the three categories of disruptions in robustness testing. In module M3, add a synthetic +12 mV voltage offset for five hours. The health estimate is within 0.5% of the reference once the offset is removed, and the suggested filter raises the innovation score without permanently lowering health. Randomly eliminate 10% of the temperature samples, and then use the last valid rack-level temperature for the temperature-normalised stress term; just slightly increase the health mean absolute error from 1.18% to 1.29%. A fast change from 0.2C charge to 1.0C discharge creates a covariance inflation ratio of 2.7 for 14 samples, which then declines, and so a single transient is not deemed a false deterioration event. Such transients can explain most residual-based alerts if covariance is constant, according to comparable station investigations [30].

The effectiveness of the state-space refinement is explained by the internal diagnostic. Figure 5 shows dynamic behaviour: Figure 5 (a) is a typical 72-hour health trajectory of module M6, and the proposed filter tracks the reference decline from 96.8% to 95.9% with a maximum deviation of 1.7%; Figure 5 (b) shows the innovation score, which has a median of 0.94 and a 99th percentile of 6.8 during dispatch switching; and Figure 5 (c) is a covariance-inflation event map, where 83% of inflation events occur under the current magnitude above 0.55C. Thus, it can be inferred from this data that when a station is not idle, a model is employed to extract degradation information from voltage residuals.

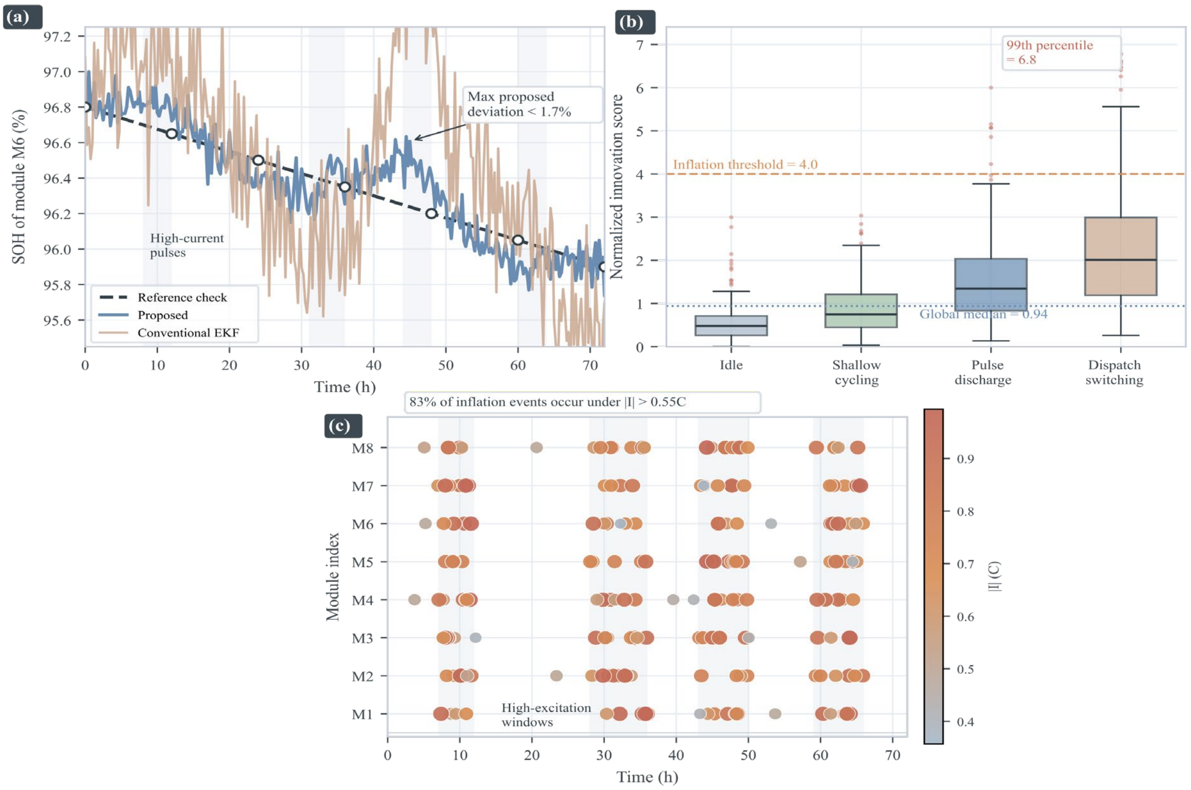


**Figure 5.** Placeholder for dynamic robustness: (a) 72 h SOH trajectory; (b) innovation-score box-and-whisker; (c) covariance-inflation event raster.

Ablation studies demonstrate the model's performance in the absence of specific components. The mean absolute error rises from 1.18% to 1.63% when the resistance-health coupling is ignored. The amount is 1.71% during high-current operation if innovation-governed covariance inflation is not subtracted. The worst-module error will rise from 1.45% to 1.88% if the module consistency restriction is eliminated because of a greater residual variation in the warm rack. The warm-rack inaccuracy rises by 0.42 percentage points when the temperature-normalized stress factor is omitted. The findings suggest that state-space improvements, as opposed to post-processing modifications, should be made to the health estimation of energy storage systems. Although the proposed formulation limits adaptability to narrow areas of damage, prior work in adaptive filtering has also demonstrated good robustness [31].

To determine how much damage each station does, ablation tests can be conducted. On a cold day, the error is increased by 0.38% when covariance inflation is excluded, but the error is changed by less than 0.1% when temperature normalization is excluded. The temperature-normalized profile of the same current will show a greater voltage drop and a quicker increase in resistance on a warm day. The module consistency requirement is required when a specific rack has consistently run-hot circumstances, but it has little impact if all modules are equally. According to the findings, the estimator is the outcome of multiple mild restrictions being activated under various operating conditions rather than a single universal corrective.

**Engineering Interpretation and Deployment Implications**

A maintenance decision can be made using some of the estimator's indicators. On day 187, Module M6, which is located in the warmest rack, fell below the 94% SOH thresholdfollowing the addition of the new filter. On day 204, the standard capacity test will be carried out. The recursive least squares baseline oscillates about the threshold for 11 days after the conventional filter sets the threshold on day 199. As a result, the suggested approach is more stable and roughly 17 days earlier. It will be used to convert regular station data into a continuous health signal for operators to compare at the rack level rather than to forecast the far future. The operating interpretation is shown in Figure 6: Figure 6 (a) maps rack-level health on day 214, with M6 at 91.9% and M2 at 95.7%; Figure 6 (b) plots temperature-health slope, with an additional monthly health loss of 0.19

percentage points for every 1°C increase; and Figure 6 (c) displays the alarm-lead-time distribution, with a median lead of 13 days over the four threshold events.

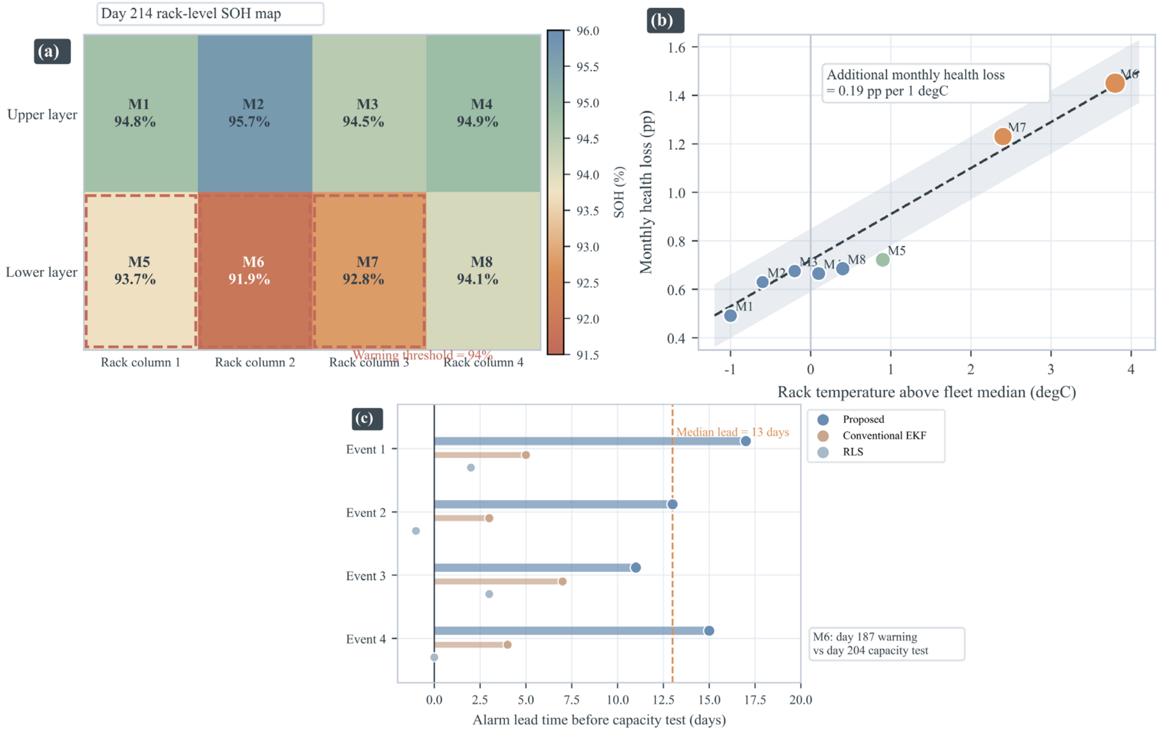


**Figure 6.** Placeholder for engineering interpretation: (a) rack-level SOH heat map; (b) temperature-health slope scatter; (c) alarm-lead-time distribution.

For station placement, the computational cost is quite low. At a 1-second sampling interval, the average update time per module on an industrial controller-class CPU is 0.37 ms; the dual Kalman baseline is 0.42 ms longer because of a different parameter filter. Covariance matrices account for the majority of memory usage, and each of the eight modules is smaller than 80 kB. Because a fifth-order fitting function may approach the open-circuit-voltage curve in the operational zone, calculating the Jacobian is rather easy. Neural network inference, a historical sequence buffer, or a cloud connection are not required. This feature is essential for station situations where a battery management system's predictable behavior during communication loss is required [32].

Additionally, the estimator works with the standard battery management system data pipeline. Because the stress term varies gradually, temperature can be updated more slowly while voltage and current reach the filter at the module sampling rate. Save the health output as an event log for covariance inflation, a rolling confidence interval, and a daily statistic. Separate the data to reduce database load; maintenance dashboards can provide hourly or daily health summaries, and short-term filtering only requires the first 1s of a stream. If one-minute summaries are preserved, the same solution would require roughly 11 MB of daily health and diagnostic storage in a station with 240 modules, which is rather little compared to raw waveform storage.

Conduct sensitivity analysis for the consistency coefficient rho, covariance inflation coefficient beta, and health weight $\lambda_Q$. The maximum accuracy is attained at $\lambda_Q$ = 0.72, meaning that resistance growth still influences power-related degradation but capacity fading accounts for the largest percentage of health definition. The model responds to high-current aging data too slowly when beta is less than 0.15; excessive health movement is caused by voltage transients when beta is more than 0.55. 0.35 is an excellent option because it is stable across all modules. For a comparatively small separation of weak modules, set the consistency coefficient rho to 0.08. Excessive covariance regulation may lose physical interpretability, and parameter ranges of this size are appropriate for practical tuning of adaptive filters [33].

The sensitivity and uncertainty are displayed in Figure 7: Figure 7 (a) the response surface of mean absolute error versus beta and rho, where the minimum region is between 0.30 and 0.42 for beta and between 0.05 and 0.11 for rho; Figure 7 (b) the calibration curve of estimated health against reference capacity checks, with a slope of 0.982 and an intercept of 1.11 percentage points; Figure 7 (c) the uncertainty bands for the last 30 days, where 92.6% of the reference points fall within the predicted 95% interval. The adoption of maintenance cannot be overconfidently encouraged by an estimator that merely provides a point value [34].

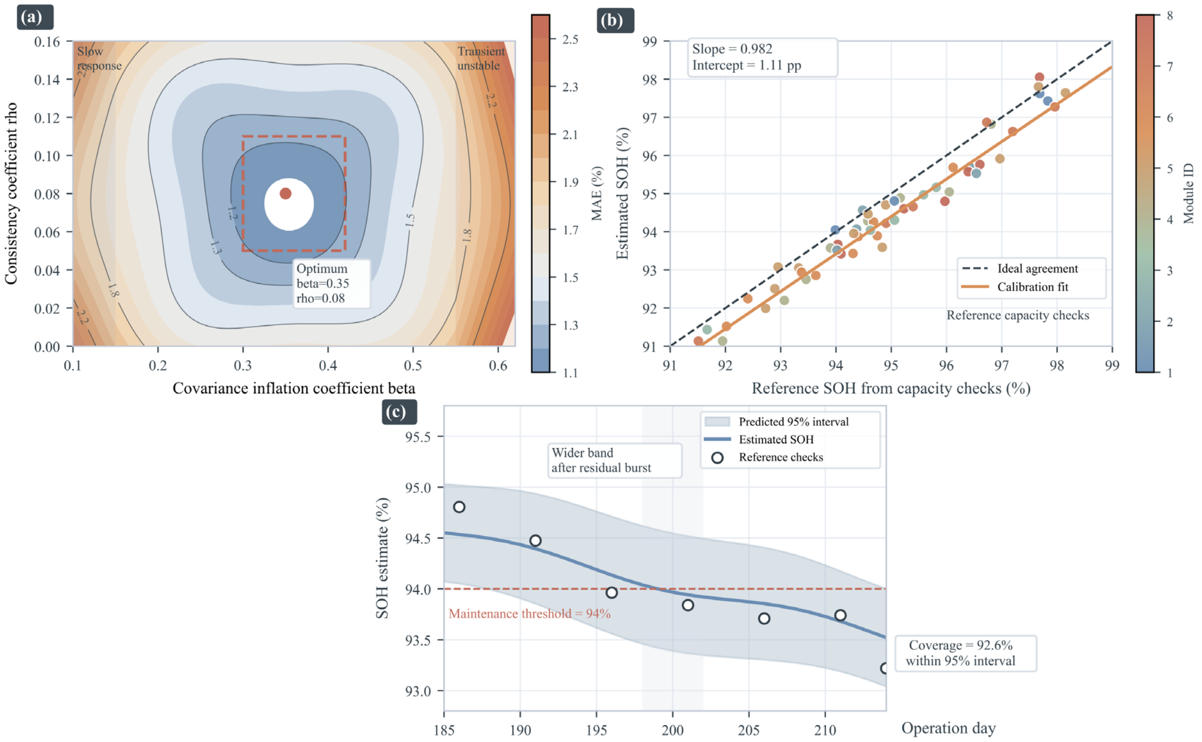


**Figure 7.** Placeholder for sensitivity and uncertainty: (a) beta-rho response surface contour; (b) SOH calibration scatter; (c) final-30-day uncertainty-band.

The enhanced filter's three engineering goals are listed below. The first is early weak-module screening, and it's important to discern between a transient voltage residual and a slight but persistent divergence. The second is thermal-risk tracking, which means that racks that age more quickly under the same dispatch can be identified using the stress-normalized drift term. Thirdly, planning for maintenance: It may be necessary to do planned catch-up work, capacity reduction, or module replacement if there is a gradual loss in health. The model should have an acceptable current-sensing calibration and a proper open-circuit-voltage curve. The parameters must be re-identified prior to deployment if the station is modified in terms of cell chemistry, capacity rating, module architecture, etc. Health models may become less accurate when both chemistry and operating conditions change at the same time, according to research on the transferability of battery diagnostics [35].

The offline determination of the open-circuit-voltage curve and nominal resistor-capacitor parameters from commissioning data would be the first step toward a workable deployment sequence. After then, the filter can operate in observation mode for a few weeks. During this time, health estimates won't be compared to planned capacity checks or set off alarms. Instead of using a single point estimate, operators can activate warning rules based on health level, health slope, and uncertainty width after the first validation interval. The likelihood of a first-run parameter mismatch necessitating intervention is decreased by staged deployment. Additionally, it gives engineers a transparent record of how the health estimate varies with residuals in voltage, current, and temperature.

Additionally, there are several interpretation flaws in the experiment. Short-term mistakes between checks cannot be properly validated since the reference health labels are based on sporadic low-current capacity checks rather than continuous ground facts. The data spans 214 days; end-of-life behavior around 80% health has not yet been documented, while early decline in the visible light domain is available. The technique has been used for lithium iron phosphate modules, and because to differences in their voltage plateau and temperature response, nickel-rich cells would require differing resistance-health weights. The decreased mean absolute error, a lower 95th percentile error, and an early warm-rack warning demonstrate that state-space refinement is possible for station-level health estimate despite the shortcomings. Currently, long-duty-cycle field validation is also required for engineering standardization [36].

## Conclusion

In this research, a state-space refined Kalman filter model for battery state-of-health estimation in energy storage power plants is developed. Incorporate capacity, resistance, and health into the recursive state vector, link them to a second-order equivalent-circuit voltage equation, and use innovation statistics to control degradation-state uncertainty. The construction is very straightforward and satisfies the power system's realistic needs for current pulsation and partial load cycling.

The research is not flawless. Reference health values are obtained through periodic capacity testing rather than continuous monitoring, and only one LiFePO4 station-like dataset is used for validation. The model is appropriate for voltage-residual analysis because it also depends on a calibrated open-circuit-voltage relationship and sensor quality. The study's generalizability may be diminished if battery chemistry, module topology, and station control technique are altered.

The technique will be expanded in the future to include pack-level balancing interactions, multiple-chemistry storage systems, and longer-term field records. Station operators can update aging characteristics across numerous sites while preserving the physical meaning of the health state by combining the existing interpretable filter with uncertainty-aware fleet learning. The alternative is to link the estimator to maintenance optimization and utilize the health uncertainty to modify replacement schedules and inspection cycles.

**Author Contributions**

Adam Kacper Dmochowski contributes to conceptualization, methodology, software, validation, analysis, investigation, data collection, draft preparation, manuscript editing, visualization, supervision, project administration, and funding acquisition. Ludwik Kostecki contributes to validation and investigation. All authors have read and agreed with the manuscript before its submission and publication.

**Funding**

This research received no specific financial support from any funding agency.

**Institutional Review Board Statement**

Not applicable.

## References

[1] Edge, J. S., O'Kane, S., Prosser, R., Kirkaldy, N. D., Patel, A. N., Hales, A., ... & Offer, G. J. (2021). Lithium ion battery degradation: what you need to know. Physical Chemistry Chemical Physics, 23(14), 8200-8221. https://doi.org/10.1039/d1cp00359c

[2] Roman, D., Saxena, S., Robu, V., Pecht, M., & Flynn, D. (2021). Machine learning pipeline for battery state-of-health estimation. Nature Machine Intelligence, 3(5), 447-456. https://doi.org/10.1038/s42256-021-00312-3 https://doi.org/10.1038/s42256-021-00312-3

[3] Li, W., Sengupta, N., Dechent, P., Howey, D., Annaswamy, A., & Sauer, D. U. (2021). Online capacity estimation of lithium-ion batteries with deep long short-term memory networks. Journal of Power Sources, 482, 228863. https://doi.org/10.1016/j.jpowsour.2020.228863

[4] Naseri, F., Schaltz, E., Stroe, D. I., Gismero, A., & Farjah, E. (2022). An Enhanced Equivalent Circuit Model With Real-Time Parameter Identification for Battery State-of-Charge Estimation. IEEE Transactions on Industrial Electronics, 69(4), 3743-3751. https://doi.org/10.1109/tie.2021.3071679

[5] Li, W., Rentemeister, M., Badeda, J., Jöst, D., Schulte, D., & Sauer, D. U. (2020). Digital twin for battery systems: Cloud battery management system with online state-of-charge and state-of-health estimation. Journal of Energy Storage, 30, 101557. https://doi.org/10.1016/j.est.2020.101557

[6] Li, J., Ye, M., Gao, K., Xu, X., Wei, M., & Jiao, S. (2021). Joint estimation of state of charge and state of health for lithium-ion battery based on dual adaptive extended Kalman filter. International Journal of Energy Research, 45(9), 13307-13322. https://doi.org/10.1002/er.6658

[7] He, Z., Yang, Z., Cui, X., & Li, E. (2020). A Method of State-of-Charge Estimation for EV Power Lithium-Ion Battery Using a Novel Adaptive Extended Kalman Filter. IEEE Transactions on Vehicular Technology, 69(12), 14618-14630. https://doi.org/10.1109/tvt.2020.3032201

[8] Zhu, R., Duan, B., Zhang, J., Zhang, Q., & Zhang, C. (2020). Co-estimation of model parameters and state-of-charge for lithium-ion batteries with recursive restricted total least squares and unscented Kalman filter. Applied Energy, 277, 115494. https://doi.org/10.1016/j.apenergy.2020.115494

[9] Shu, X., Li, G., Shen, J., Lei, Z., Chen, Z., & Liu, Y. (2020). An adaptive multi-state estimation algorithm for lithium-ion batteries incorporating temperature compensation. Energy, 207, 118262. https://doi.org/10.1016/j.energy.2020.118262

[10] Tran, M. K., DaCosta, A., Mevawalla, A., Panchal, S., & Fowler, M. (2021). Comparative Study of Equivalent Circuit Models Performance in Four Common Lithium-Ion Batteries: LFP, NMC, LMO, NCA. Batteries, 7(3), 51. https://doi.org/10.3390/batteries7030051

[11] Zhou, W., Zheng, Y., Pan, Z., & Lu, Q. (2021). Review on the Battery Model and SOC Estimation Method. Processes, 9(9), 1685. https://doi.org/10.3390/pr9091685

[12] Zhang, S., Guo, X., Dou, X., & Zhang, X. (2020). A rapid online calculation method for state of health of lithium-ion battery based on coulomb counting method and differential voltage analysis. Journal of Power Sources, 479, 228740. https://doi.org/10.1016/j.jpowsour.2020.228740

[13] Jiang, B., Zhu, J., Wang, X., Wei, X., Shang, W., & Dai, H. (2022). A comparative study of different features extracted from electrochemical impedance spectroscopy in state of health estimation for lithium-ion batteries. Applied Energy, 322, 119502. https://doi.org/10.1016/j.apenergy.2022.119502

[14] Hosseininasab, S., Lin, C., Pischinger, S., Stapelbroek, M., & Vagnoni, G. (2022). State-of-health estimation of lithium-ion batteries for electrified vehicles using a reduced-order electrochemical model. Journal of Energy Storage, 52, 104684. https://doi.org/10.1016/j.est.2022.104684

[15] Stroe, D. I., & Schaltz, E. (2020). Lithium-Ion Battery State-of-Health Estimation Using the Incremental Capacity Analysis Technique. IEEE Transactions on Industry Applications, 56(1), 678-685. https://doi.org/10.1109/tia.2019.2955396

[16] Zhang, S., Guo, X., & Zhang, X. (2020). An improved adaptive unscented kalman filtering for state of charge online estimation of lithium-ion battery. Journal of Energy Storage, 32, 101980. https://doi.org/10.1016/j.est.2020.101980

[17] Jiang, C., Wang, S., Wu, B., Fernandez, C., Xiong, X., & Coffie-Ken, J. (2021). A state-of-charge estimation method of the power lithium-ion battery in complex conditions based on adaptive square root extended Kalman filter. Energy, 219, 119603. https://doi.org/10.1016/j.energy.2020.119603

[18] Sun, D., Yu, X., Wang, C., Zhang, C., Huang, R., Zhou, Q., Amietszajew, T., & Bhagat, R. (2021). State of charge estimation for lithium-ion battery based on an Intelligent Adaptive Extended Kalman Filter with improved noise estimator. Energy, 214, 119025. https://doi.org/10.1016/j.energy.2020.119025

[19] Lin, M., Wu, D., Meng, J., Wu, J., & Wu, H. (2022). A multi-feature-based multi-model fusion method for state of health estimation of lithium-ion batteries. Journal of Power Sources, 518, 230774. https://doi.org/10.1016/j.jpowsour.2021.230774

[20] dos Reis, G., Strange, C., Yadav, M., & Li, S. (2021). Lithium-ion battery data and where to find it. Energy and AI, 5, 100081. https://doi.org/10.1016/j.egyai.2021.100081

[21] Vidal, C., Malysz, P., Kollmeyer, P., & Emadi, A. (2020). Machine Learning Applied to Electrified Vehicle Battery State of Charge and State of Health Estimation: State-of-the-Art. IEEE Access, 8, 52796-52814. https://doi.org/10.1109/access.2020.2980961

[22] Feng, J., Cai, F., Yang, J., Wang, S., & Huang, K. (2022). An Adaptive State of Charge Estimation Method of Lithium-ion Battery Based on Residual Constraint Fading Factor Unscented Kalman Filter. IEEE Access, 10, 44549-44563. https://doi.org/10.1109/access.2022.3170093

[23] Shi, N., Chen, Z., Niu, M., He, Z., Wang, Y., & Cui, J. (2022). State-of-charge estimation for the lithium-ion battery based on adaptive extended Kalman filter using improved parameter identification. Journal of Energy Storage, 45, 103518. https://doi.org/10.1016/j.est.2021.103518

[24] Gabbar, H., Othman, A., & Abdussami, M. (2021). Review of Battery Management Systems (BMS) Development and Industrial Standards. Technologies, 9(2), 28. https://doi.org/10.3390/technologies9020028

[25] Cong, X., Zhang, C., Jiang, J., Zhang, W., & Jiang, Y. (2020). A Hybrid Method for the Prediction of the Remaining Useful Life of Lithium-Ion Batteries With Accelerated Capacity Degradation. IEEE Transactions on Vehicular Technology, 69(11), 12775-12785. https://doi.org/10.1109/tvt.2020.3024019

[26] Liu, K., Shang, Y., Ouyang, Q., & Widanage, W. D. (2021). A Data-Driven Approach With Uncertainty Quantification for Predicting Future Capacities and Remaining Useful Life of Lithium-ion Battery. IEEE Transactions on Industrial Electronics, 68(4), 3170-3180. https://doi.org/10.1109/tie.2020.2973876

[27] Chen, D., Hong, W., & Zhou, X. (2022). Transformer Network for Remaining Useful Life Prediction of Lithium-Ion Batteries. IEEE Access, 10, 19621-19628. https://doi.org/10.1109/access.2022.3151975

[28] Yang, S., Zhang, C., Jiang, J., Zhang, W., Zhang, L., & Wang, Y. (2021). Review on state-of-health of lithium-ion batteries: Characterizations, estimations and applications. Journal of Cleaner Production, 314, 128015. https://doi.org/10.1016/j.jclepro.2021.128015

[29] Liu, J., Duan, Q., Qi, K., Liu, Y., Sun, J., Wang, Z., & Wang, Q. (2022). Capacity fading mechanisms and state of health prediction of commercial lithium-ion battery in total lifespan. Journal of Energy Storage, 46, 103910. https://doi.org/10.1016/j.est.2021.103910

[30] Yu, Y., Vincent, T., Sansom, J., Greenwood, D., & Marco, J. (2022). Distributed internal thermal monitoring of lithium ion batteries with fibre sensors. Journal of Energy Storage, 50, 104291. https://doi.org/10.1016/j.est.2022.104291

[31] Zhu, F., & Fu, J. (2021). A Novel State-of-Health Estimation for Lithium-Ion Battery via Unscented Kalman Filter and Improved Unscented Particle Filter. IEEE Sensors Journal, 21(22), 25449-25456. https://doi.org/10.1109/jsen.2021.3102990

[32] Liu, S., Dong, X., Yu, X., Ren, X., Zhang, J., & Zhu, R. (2022). A method for state of charge and state of health estimation of lithium-ion battery based on adaptive unscented Kalman filter. Energy Reports, 8, 426-436. https://doi.org/10.1016/j.egyr.2022.09.093

[33] Imran, R. M., Li, Q., & Flaih, F. M. F. (2020). An Enhanced Lithium-Ion Battery Model for Estimating the State of Charge and Degraded Capacity Using an Optimized Extended Kalman Filter. IEEE Access, 8, 208322-208336. https://doi.org/10.1109/access.2020.3038477

[34] Wu, J., Liu, X., Meng, J., & Lin, M. (2021). Cloud-to-edge based state of health estimation method for Lithium-ion battery in distributed energy storage system. Journal of Energy Storage, 41, 102974. https://doi.org/10.1016/j.est.2021.102974

[35] Wang, Z., Song, C., Yuan, C., & Li, X. (2021). A flexible method for state-of-health estimation of lithium battery energy storage system. Energy Reports, 7, 6375-6383. https://doi.org/10.1016/j.egyr.2021.09.054

[36] Li, Y., Stroe, D. I., Cheng, Y., Sheng, H., Sui, X., & Teodorescu, R. (2021). On the feature selection for battery state of health estimation based on charging–discharging profiles. Journal of Energy Storage, 33, 102122. https://doi.org/10.1016/j.est.2020.102122